



## Passive water removal in fuel cells by capillary droplet actuation

Tobias Metz<sup>a,\*</sup>, Nils Paust<sup>a</sup>, Claas Müller<sup>b</sup>, Roland Zengerle<sup>a</sup>, Peter Koltay<sup>a</sup>

<sup>a</sup> *Laboratory for MEMS Applications, Department of Microsystems Engineering (IMTEK), University of Freiburg, Georges-Koehler-Allee 106, D-79110 Freiburg, Germany*

<sup>b</sup> *Laboratory for Process Technology, Department of Microsystems Engineering (IMTEK), University of Freiburg, Georges-Koehler-Allee 106, D-79110 Freiburg, Germany*

Received 10 April 2007; received in revised form 18 June 2007; accepted 26 June 2007

### Abstract

In this paper, a microstructured flow field for passive water management in proton exchange membrane fuel cells (PEMFC) is presented. It is based on the transport of liquid water droplets by capillary forces. A triangular microchannel forces droplets to detach from a fuel cell's gas diffusion layer (GDL) or membrane electrode assembly (MEA). Thus, it ensures proper oxygen supply of the reactive area. Water droplets are lifted into a secondary channel, and removed from the fuel cell by capillary action. Water formation in the flow field channels has been studied by analytic models and experiments. Three droplet configurations were identified, which show different properties in terms of capillary transport. Preferred shapes cover the GDL only slightly and can be found for contact angles typical for fuel cell materials. The actuation mechanism was studied by simulations for different designs, with varying contact angles and geometries. The new channel design was compared in a test fuel cell to standard rectangular channels, in the initial phase of the cell, at low working temperatures (22–30 °C). The new flow field design stabilized the cell at 95% of its initial performance compared to 60% when using the standard design.

© 2007 Elsevier B.V. All rights reserved.

**Keywords:** Fuel cell; Canthotaxis; Water management; Capillary action; PEMFC; Channel clogging; Droplet

### 1. Introduction

This work deals with a major challenge in PEM fuel cell design: removal of abundant water from the cathode. Water is produced in fuel cell cathodes by the oxidation of protons. On the one hand, it is essential for the operation. It enables the proton transport in the membrane, and is part of the cathode reaction. On the other hand, too much water disturbs the operation. In the low temperature range (20–65 °C), up to 95% of water is present in liquid phase [1]. In conventional flow fields, water can block channels and inhibit proper oxygen supply. Parallel channels, driven by a common pressure source, suffer from a sustainable performance decline if individual channels are clogged by process water. The channels cannot be reopened by the gas flow, as there is a lower resistance through the open channels [2,3].

Today's common approach is to have a low number of channels in a meandering arrangement. This allows for the removal of water by purging the cathode flow field [4], but high flow rates are required to ensure a sufficient distribution of oxygen along the extended channels [5,6]. High pressure-gradients and special strategies like periodically purging the channel system are necessary. Furthermore, it has been shown, e.g. in refs. [5,6] that long channels lead to inhomogeneous humidification conditions and a resulting non-optimal power generation. As a consequence, the membrane dries out at the beginning of the system and liquid accumulates at the channel ends.

In order to improve water management in PEMFC, a passive approach to remove the abundant water from the cathode by capillary forces is presented in the following. Capillary forces have been considered in the context of fuel cells for the removal of gas bubbles from the anode of direct methanol fuel cells (DMFC) [7]. Shape and formation of droplets in flow field channels of PEMFC were discussed in ref. [4] where a similar behaviour of droplets like in this work could be observed. Nevertheless, in ref. [4] standard square channels were studied without optimization for liquid transport. In this configuration, the droplet

\* Corresponding author at: IMTEK – University of Freiburg, Lab for MEMS Applications, Georges-Koehler-Allee 103, D-79110 Freiburg, Germany.  
Tel.: +49 761 203 7325/7476; fax: +49 761 203 7312/7539.  
E-mail address: [tmetz@imtek.de](mailto:tmetz@imtek.de) (T. Metz).

removal works only for very hydrophilic channel walls. At high gas flow rates, the resulting annular liquid distribution leads to the formation of water lenses, which again induces a high flow resistance. To avoid this, channels with tapered walls are proposed in this work. These channels separate the liquid by capillary forces from the gaseous flow, perpendicular to the main gas flow direction. The concept ensures air supply even if a large amount of water is produced. The channel is designed to force liquid to spread in a secondary channel at top of the tapered section. This supports a proper distribution of water throughout the cell. The channel geometry is similar to the channel design presented for the separation of gas bubbles in microchannels in ref. [8]. The new channel design has been presented first in ref. [9]. Here, we provide a more detailed discussion of the working principle, including further topics like contact angle dynamics and show additional experimental results.

In the first part of this work, the working principle of the new channel design is explained. It discusses wetting conditions and droplet formation. The second part shows simulations performed with computational fluid dynamics (CFD). They are used to study the droplet movement in different channel geometries. In the third part, experiments with channels artificially filled with water are presented as well as results obtained during operation in a fuel cell.

## 2. Working principle

### 2.1. Channel setup

The proposed flow field consists of parallel channels with a cross-section as depicted in Fig. 1. The channel walls are tapered perpendicular to the flow direction with their wider end towards the MEA or GDL. At the narrow end, the channel descends into a rectangular secondary channel (C) with width  $w$  and depth  $d$ . The surfaces of the flow field channels are considered to be hydrophilic. The MEA or GDL of the fuel cell seals the channels at the bottom and exhibits a hydrophobic surface.

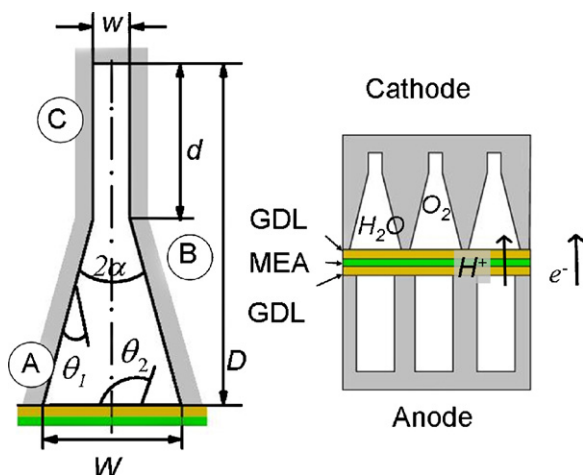


Fig. 1. Schematic of the channel design (left) and integration into a PEMFC assembly (right).

### 2.2. Droplet actuation

In Fig. 2, the results of a CFD simulation are shown to visualize the working principle. The pictures show a view along the channel axis. The mechanism of droplet removal from the MEA/GDL will be explained here in context of this result.

In Fig. 2(a), a droplet is growing at the bottom of the channel where the hydrophobic MEA/GDL is placed. Water is generated in fuel cells in the catalytic layer between MEA and GDL. The liquid follows given paths through the GDL [1]. At the positions where these paths reach the open channel, the growth of droplets can be observed [4].

Droplets can grow at any position in the channel (Fig. 2(a)). Nevertheless, when a droplet is large enough it meets one of the wetting channel walls and moves there immediately, attracted by capillary forces (Fig. 2(b)). From this moment, the situation is the same as if the droplet grows at the channel wall. Droplets continue growing by drain of water through the GDL or by merging with neighbouring droplets (Fig. 2(c)). As soon as a droplet is large enough to touch the opposite channel wall as well, it is pulled towards it (Fig. 2(d)). At this point the droplet has reached the maximum size, feasible in the tapered channel. Therefore, this size will be referred to as critical droplet size. The larger the critical droplet size is, the smaller is the rate of droplet removal. The critical droplet size depends on the wetting conditions and channel geometry.

After overcoming the critical size (Fig. 2(e)), the droplet gets sucked towards the narrow end of the channel. For a very short time (less than 50 ms in the simulation), the whole channel cross-section can be blocked (Fig. 2(f)). Droplet movement towards the narrow channel end leads to a clearing of the wider part of the channel (Fig. 2(g)).

In the simulation shown in Fig. 2, water generation was mimicked by a constant mass flow rate, feeding the droplet from a small zone at the bottom of the channel. While the first droplet leaves the MEA/GDL completely, a second droplet already grows (Fig. 2(h)) and the mechanism is repeated. In the long run when no more liquid is produced, only the upper channel is liquid filled (Fig. 2(i)). From there, the liquid can be drained out of the fuel cell by capillary forces in non-woven material provided at the end of the channels.

### 2.3. Influence of gravity

The influence of gravity on the described process can be estimated by the Bond number  $Bo$  [10]. It compares the capillary pressure with the hydrostatic pressure. For the tapered channel like depicted in Fig. 1, the Bond number is calculated in a vertical setup as follows:

$$Bo = \frac{\rho g(D - d)}{\sigma \cos\theta_1(1/w - 1/W)} \quad (1)$$

The largest value for channels considered in this work is  $Bo = 0.49$ . It relates to a channel with  $W = 1100 \mu\text{m}$ ,  $w = 300 \mu\text{m}$ ,  $D - d = 3000 \mu\text{m}$  and  $\theta_1 = 70^\circ$ . In all other cases, the Bond number has been smaller than 0.35. Thus, gravity plays a negligible role.

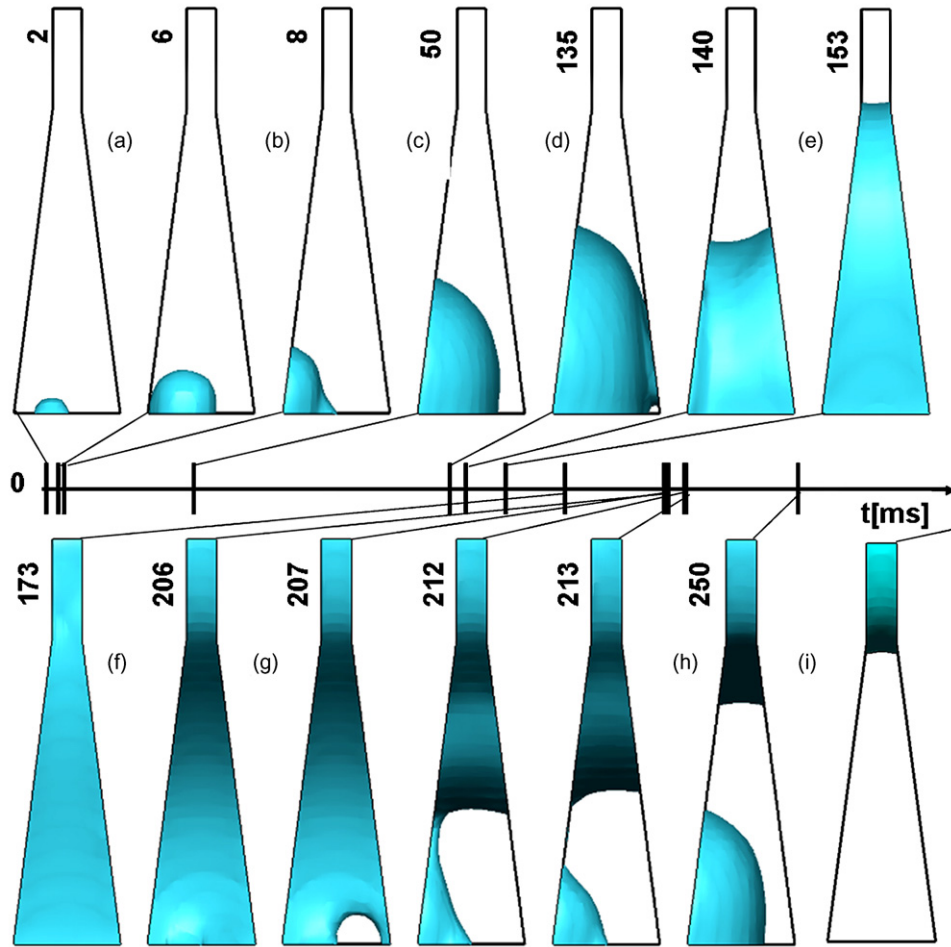


Fig. 2. Mechanism of droplet removal in tapered channel: (a) droplet growth; (b) droplet moves to wetting wall; (c) further growth of droplet; (d) droplet meets second wall; (e) droplet is elongated towards upper channel; (f) filled cross-section; (g) uplift frees cross-section; (h) droplet is nearly lifted while second droplet already starts growth; (i) when liquid generation is stopped after growth, liquid resides only in the upper channel. (CFD simulation:  $\theta_2 = 105^\circ$ ,  $\theta_1 = 70^\circ$ ,  $W = 1100 \mu\text{m}$ ,  $D = 4000 \mu\text{m}$ ,  $w = 300 \mu\text{m}$ ,  $2\alpha = 15^\circ$ ).

#### 2.4. Droplet shapes

Without loss of generality, droplets can be considered to reside at the edges where hydrophobic and hydrophilic walls meet (Fig. 1, detail A), at some moment in time. For such droplets sitting in an edge, only two principal surface geometries are possible [11]. The droplet has either a spherical shape, cut off by the channel walls (Fig. 3(b and c)) or the shape of an infinite cylinder (Fig. 3(a)). This results from the constant capillary

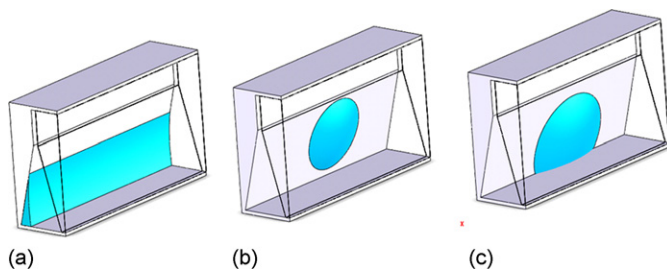


Fig. 3. Attainable modes for droplet shapes: (a) edge mode; (b) wall mode; (c) droplet mode.

pressure of the droplet, which requires an interface of constant curvature.

Depending on contact and opening angles, only three different shape modes can be attained by the droplets (Fig. 3). These modes will be referred to as edge mode, wall mode and droplet mode. Only the wall mode and droplet mode enable the capillary actuated movement of droplets like described before.

The actual droplet shape can be predicted by the theory of Canthotaxis as given in ref. [11]. The results are displayed in Fig. 4 for the specific situation encountered in a PEMFC: every point in Fig. 4 corresponds to a pair of contact angles  $\theta_1$ ,  $\theta_2$  where the contact angle on the channel walls is denoted as  $\theta_1$  and the contact angle at the MEA is denoted as  $\theta_2$ . Straight lines separate the regions where different droplet shapes are attained. The various lines displayed in different grey levels correspond to half opening angles of  $\alpha = 0^\circ$ ,  $15^\circ$  and  $30^\circ$  of the channel.

In the edge mode, the liquid spreads along the edge as depicted in Fig. 3(a). This mode is defined by the condition:

$$\theta_1 + \theta_2 < \alpha + \frac{\pi}{2} \quad (2)$$

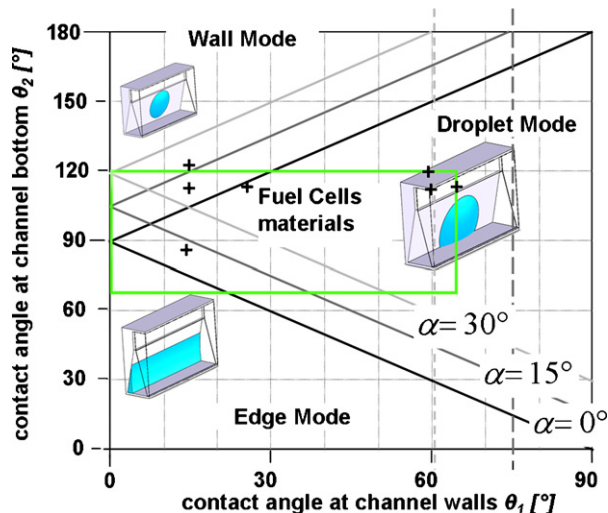


Fig. 4. Attainable modes for droplet shapes as a function of contact angles for opening angles  $\alpha = 0^\circ$ ,  $15^\circ$  and  $30^\circ$ . Realistic contact angle values for fuel cells are marked by a rectangle. The situations in the experiments and the CFD simulation are marked by a cross ( $\alpha = 15^\circ$  and  $7.5^\circ$ ). The dashed line marks the Concus–Finn condition.

In Eq. (2),  $\alpha$  again denotes half the opening angle of the channel walls. The parameters for which the edge mode is achieved can be found in the lower left corner of Fig. 4.

The wall mode (Fig. 3(b)) is attained for a very high difference in the wetting conditions of GDL and channel walls. In this configuration, the droplet does not wet any part of the GDL. The corresponding equation is:

$$\theta_2 > \theta_1 + \alpha + \frac{\pi}{2}. \quad (3)$$

Between these extreme conditions, the droplets reside in the channel like shown in (Fig. 3(c)) which is referred to as droplet mode. The defining inequality is given by combination of Eqs. (2) and (3):

$$\theta_2 - \alpha + \frac{\pi}{2} > \theta_1 > \alpha + \frac{\pi}{2} - \theta_2 \quad (4)$$

In the droplet mode, the GDL is partly wetted and the liquid stays compact in a spherical shape (Fig. 3(c)).

Droplet and wall mode are spherical surfaces, which intercept the walls with the associated contact angles. In principal, cylindrical surfaces are possible in these cases as well, but are unstable and break into droplets immediately, having smaller interfacial energies [11,12].

### 2.5. Concus–Finn condition

Droplets move only completely away from the MEA and spread along the secondary channel if the Concus–Finn condition [13] is fulfilled, i.e.

$$\theta_1 + \alpha < \frac{\pi}{2} \quad (5)$$

If Eq. (5) is fulfilled, the tapered channel is a so-called critical edge. When the channel walls are hydrophilic ( $\theta_1 < 90^\circ$ ), the droplets move upwards in any case. However, if Eq. (5) is not fulfilled,

they stay above their initial position and accumulate—in the worst case until the channel is clogged. The dashed vertical lines in Fig. 4 denote the condition for the opening angles  $\alpha = 15^\circ$  and  $\alpha = 30^\circ$ . For  $\alpha = 0^\circ$ , the condition given at  $\theta_1 = 90^\circ$ .

### 2.6. Relevance for PEMFC

The shape modes that can be attained in fuel cells obviously depend on the surface properties of the materials. In Fig. 4, typical contact angle values, obtained for typical fuel cell materials, are surrounded by a rectangle in the centre of the plot. For example, an often used electrode material in fuel cells is graphite that exhibits contact angles of  $60\text{--}70^\circ$ . Electrodes with better wetting properties are metals like stainless steel or gold coatings. These, as well as silicon with an oxide layer on top, lead to contact angles down to  $0^\circ$ . In operation, contaminations can lower the surface energy. Together with surface roughness, this leads to increased contact angles and contact angle hysteresis. Thus, advancing contact angles must be assumed larger than the ones measured for pure materials. In Fig. 4, the contact angle range for flow field walls is assumed from  $0^\circ$  to  $70^\circ$ .

The MEA or GDL is typically treated with Teflon resulting in wetting angles up to  $120^\circ$ . In Fig. 4, the contact angle range typical for fuel cells starts at  $75^\circ$  for minor Teflon-treated carbon paper to a maximum of  $120^\circ$  for strongly fluorinated GDLs. Thus, in the majority of cases the droplet mode will be preferred in typical fuel cells and the described droplet transport mechanism should work for small values of  $\alpha$ .

### 2.7. Efficiency of uplift

The efficiency of the water removal depends strongly on the shape mode the liquid attains. The edge mode is undesired as it fills a whole channel slowly but steadily. Thus, it blocks the active GDL region near the electrodes along the whole channel from air supply. Once the liquid in edge mode builds a bridge between the opposing channel walls, it can be removed as well. As it has to be removed for the whole channel at once, it requires a large secondary channel, which must be able to buffer the immediate flow. Also, some liquid will stay in the edges, as all three edges of the triangular channel are critical in that case.

Droplet mode and in the best case wall mode are preferred conditions for the application in fuel cells, because only small areas of the GDL are blocked. The droplets are lifted into the removal channel as soon as they touch both walls. The small volume of a single droplet typically does not overstrain the capacity of the removal channel.

While the wall mode leads to zero coverage of the MEA it cannot easily be realized using standard materials. The droplet mode covers most of the parameter range typical for fuel cells and enables a reliable and local droplet removal.

### 2.8. Contact angle hysteresis and pinning

At the edge where the tapered channel descends into the narrow secondary channel the contact line can be subject of pinning like shown in Fig. 5(a). The effective contact angle, relative to the

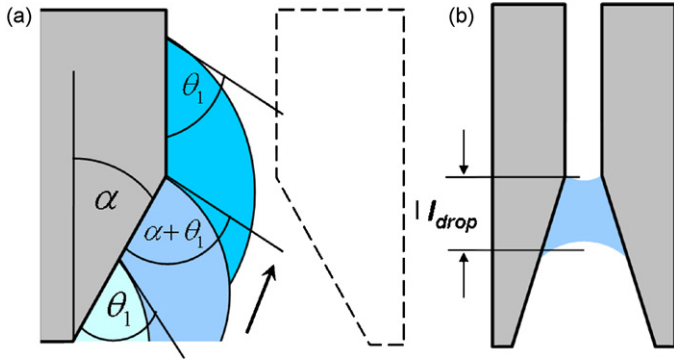


Fig. 5. (a) Contact line pinning at the edge of the secondary channel. The apparent contact angle relative to the tapered wall increases from  $\theta_1$  to  $(\theta_1 + \alpha)$ . (b) Bridge of liquid that remains in the middle of the channel due to contact angle hysteresis.

lower edge increases from  $\theta_1$  to  $(\theta_1 + \alpha)$ . Therefore, the droplet experiences some kind of resistance and slows down there.

The question arises, if a droplet can be trapped below the edge and build a bridge between the opposing walls (Fig. 5(b)). This question can be answered by assuming such a droplet with length  $l_{drop}$  like in Fig. 5(b), and comparing its capillary pressure difference between the upper and lower end of the droplet. The droplet moves if the capillary pressure drop at the upper end is higher. This leads to Eq. (6):

$$\frac{\sigma \cos \theta_1}{w} > \frac{\sigma \cos(\theta_1 + \alpha)}{(w + 2 \tan \alpha l_{drop})} \quad (6)$$

Separating the length scales and the angular arguments in Eq. (6), one obtains Eq. (7).

$$1 + 2 \tan \alpha \frac{l_{drop}}{w} > \frac{\cos(\theta_1 + \alpha)}{\cos \theta_1} \quad (7)$$

In Eq. (7), the left-hand side is always greater than one, while the right hand side is always smaller than one. Thus, the equation is always fulfilled. A liquid bridge trapped by pinning as shown in Fig. 5(b) is theoretically impossible for constant contact angles.

The situation changes, if contact angle hysteresis is taken into account. This can be done by substituting the advancing contact angle  $\theta_{1adv}$  at the edge and the lower receding contact angle  $\theta_{1adv} - \Delta\theta$  at the lower end of the droplet into Eq. (7), resulting in Eq. (8):

$$1 + 2 \tan \alpha \frac{l_{drop}}{w} > \frac{\cos(\theta_{1adv} - \Delta\theta + \alpha)}{\cos \theta_{1adv}} \quad (8)$$

For the limit of a droplet length towards zero  $l_{drop} \sim 0$ , Eq. (8) is not valid for,

$$\Delta\theta > \alpha. \quad (9)$$

Thus, if the difference between advancing and receding contact angle exceeds half the opening angle of the channel, a droplet can be trapped at the edge. Therefore, larger opening angles must be preferred, to safely prevent pinning of up moving droplets.

An advantage of pinning is that the liquid is kept from moving back into the tapered channel once it is placed in the removal channel.

### 3. Simulations

The mechanism of the passive droplet removal was studied by CFD simulations using the commercially available software package CFD-ACE+ from ESI-CFD [14]. The Navier–Stokes equations are solved by the program in combination with the volume of fluid (VOF) method, which considers the free surface between air and water. The model incorporates surface tension at the interface between liquid and gas as well, and reconstructs the contact angle at the triple line. However, only static contact angles are considered by the applied model.

Simulations were performed for the parameter sets given in Table 1. In simulations a, b and c, water compartments were predefined in the channel. They were large enough to touch the opposite channel walls.

In simulations d and e, liquid was introduced into the channel from an inlet at the bottom. The applied flow rate of  $26 \mu\text{l/s}$  corresponds to the water produced in the GDL area of a channel with length 20 mm and width  $W = 1.1 \text{ mm}$  at a constant current density of  $j = 800 \text{ mA/cm}^2$ . This is a worst-case scenario for the fabricated fuel cell assuming that all water produced is captured in one point. As a consequence, the rate of droplet growth is relatively fast (Fig. 2). The desired droplet removal has been observed in all simulations even for the low contact angle of  $85^\circ$  at the GDL.

In Table 1, removal times for single droplets are given, predicted by the simulations. They represent the time between the moments when the uplift starts until the water is completely moved into the upper channel. It can be found that the removal times for the smaller channels (a, b and c) are an order of magnitude smaller than for the larger channels (d and e). Reasons for this are the better wetting conditions and the larger opening

Table 1  
Parameter sets of performed simulations and droplet removal times of droplets after droplet removal is initiated

	$W$ ( $\mu\text{m}$ )	$w$ ( $\mu\text{m}$ )	$d$ ( $\mu\text{m}$ )	$D$ ( $\mu$ )	$2\alpha$ ( $^\circ$ )	$\theta_1$ ( $^\circ$ )	$\theta_2$ ( $^\circ$ )	$t_{lift}$ (ms)	Bo
(a)	300	100	150	550	28.1	15	85	20	0.008
(b)	300	100	150	550	28.1	15	120	15	0.008
(c)	300	130	500	817	30	30	105	15	0.01
(d)	1100	300	1000	4000	15	70	105	200	0.49
(e)	1100	300	1000	4000	15	60	110	100	0.33

The uplift time is time taken from the simulations. Simulations were performed without gravity. The Bond number was calculated according to Eq. (1) for  $g = 9.81 \text{ ms}^{-2}$ ,  $\rho = 1000$ .

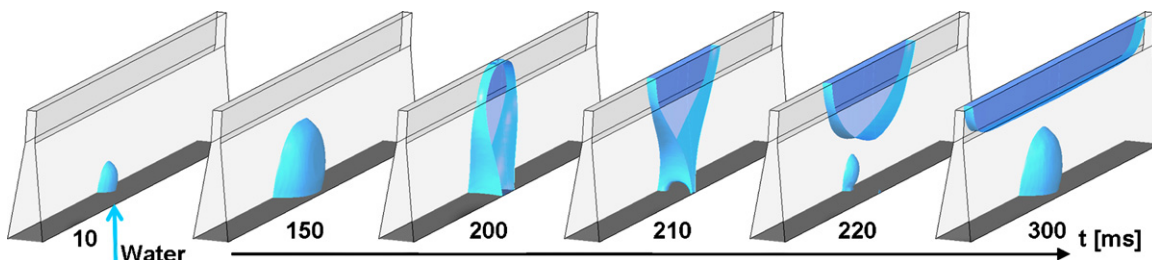


Fig. 6. CFD simulation of a droplet growing from the hydrophobic channel bottom ( $\theta_2 = 110^\circ$ ) along the channel walls ( $\theta_1 = 60^\circ$ ). As soon as the droplet touches the opposite wall, capillary forces lift the water into the upper channel (dimensions:  $W = 1100 \mu\text{m}$ ,  $D = 4000 \mu\text{m}$ ,  $w = 300 \mu\text{m}$ ,  $2\alpha = 15^\circ$ ).

angles as well as the higher capillary pressure caused by the smaller size of the channels.

The simulation results displayed in Fig. 6 show a detailed view of the growth and removal of a droplet in the simulation. When reaching the opposite wall, a liquid bridge is formed and the water is lifted. The droplet breaks up, and a small secondary droplet remains at the wall while the liquid bridge moves upwards and spreads along the secondary water removal channel.

## 4. Experiments

### 4.1. Test channels

In the first experiment, test channels with the proposed geometry were milled into transparent PMMA. The channel profile was fabricated in two steps: first, the tapered part was milled using a conical cutter with an opening angle of  $2\alpha = 30^\circ$ . In the second step, straight channels were sawed into the center of the tapered section to a depth of  $3333 \mu\text{m}$ , measured from the initial surface. The secondary channel was realized using a saw blade with a tooth width of  $150 \mu\text{m}$ .

The channels were plasma-treated to obtain a contact angle of  $\theta_1 = 20^\circ$ . Afterwards they were sealed with hydrophobic PDMS ( $\theta_2 = 105^\circ$ ). To observe the principle of droplet removal, coloured water was manually introduced into the channels through a  $200 \mu\text{m}$  pipe from the bottom of the PDMS sealing.

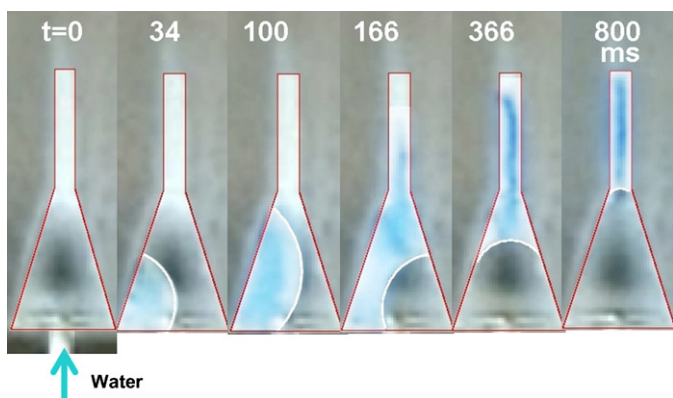


Fig. 7. A single droplet is generated by pressure-driven flow through a hole at the bottom ( $W = 1400 \mu\text{m}$ ,  $D = 3333 \mu\text{m}$ ,  $w = 150 \mu\text{m}$ ,  $\alpha = 15^\circ$ ,  $\theta_1 = 20^\circ$ ,  $\theta_2 = 105^\circ$ ,  $Bo = 0.08$ ).

Fig. 7 shows growth and removal of water in droplet mode. The droplet of approximately  $4.3 \mu\text{l}$  is removed within less than  $400 \text{ ms}$ . As expected from simulations, the droplet moves towards one wall and is lifted up when touching the opposite wall.

In Fig. 8, the same channel is flooded at a high liquid flow rate. After the inlet flow stops, the channel is cleared within  $4.3 \text{ s}$  due to capillary action. In both cases, the liquid resides only in the secondary channel after the removal process is terminated.

The experiments show that the proposed channel system indeed is able to act as a highly efficient actuator for the transport of condensed water.

### 4.2. Fuel cell fabrication

For in situ experiments, a fuel cell employing the presented channel design at the cathode was fabricated as depicted in Fig. 8. Cathode and anode (Fig. 8(a and b)) consist of graphite plates (Ringsdorff R7340 [15]) with milled channel systems for gas supply. A contact angle for water of  $60^\circ$  was measured on the materials surface. To increase the wetting behaviour, the channel walls were coated in some experiments with PEG (polyethylenglycol), resulting in a contact angle of  $\theta_1 \sim 15^\circ$ . The MEA/GDL sandwich (Fig. 8(c)) was pressed between the flow fields. The MEA used was made from Naphion® N112 with catalytic layers with  $0.3 \text{ mg/cm}^2$  platinum at the anode and  $0.6 \text{ mg/cm}^2$  at the cathode [16]. Carbon paper Sigracet 10CC [15] was used as gas diffusion layer, containing 10% weight Teflon to reach hydrophobic [16] behaviour. After this treatment, contact angles of  $105^\circ$  were measured. The design of the fuel cell as displayed

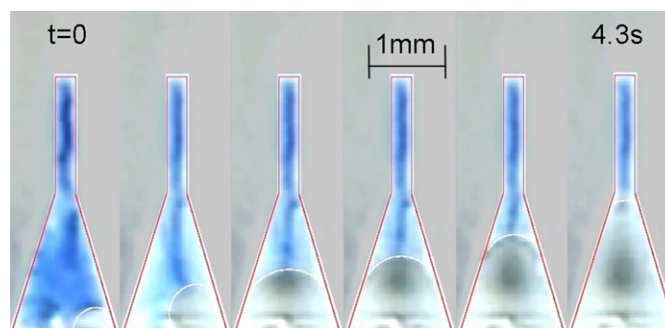


Fig. 8. A totally flooded channel is emptied from bottom to top ( $W = 1400 \mu\text{m}$ ,  $D = 3333 \mu\text{m}$ ,  $w = 150 \mu\text{m}$ ,  $\alpha = 15^\circ$ ,  $\theta_1 = 20^\circ$ ,  $\theta_2 = 105^\circ$ ,  $Bo = 0.08$ ).

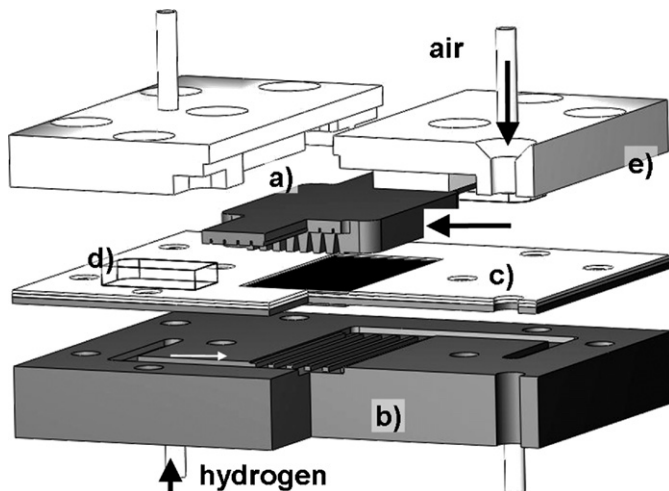


Fig. 9. Test fuel cell (cut at right front) with: (a) exchangeable cathode flow field; (b) graphite anode; (c) MEA, GDL and sealing assembly; (d) observation window; (e) polycarbonate frame.

in Fig. 9 contains a window (Fig. 9(d)), which allows for visual inspection of the cathode flow channels. Water movement in perpendicular directions to the gas flow could be observed through it (Fig. 10).

A single cathode flow field was fabricated with four channels having opening angles of  $2\alpha = 15^\circ$  (two channels),  $2\alpha = 20^\circ$  and  $2\alpha = 30^\circ$ . The total channel depth was  $D = 4000 \mu\text{m}$  in all cases with a removal channel of width  $w = 300 \mu\text{m}$  and depth  $d = 1000 \mu\text{m}$ . The fabrication process was different from the test channels in so far that the sawing was done in advance to the milling with the conical cutters, increasing the lifetime of the cutters.

Furthermore, a reference flow field for the cathode was built, having three channels with rectangular cross-sections (width,  $1000 \mu\text{m}$ ; depth,  $2320 \mu\text{m}$ ) for comparison. At the anode, standard rectangular channels were milled into the graphite for the hydrogen supply (depth,  $1 \text{ mm}$ ; width,  $2 \text{ mm}$ ).

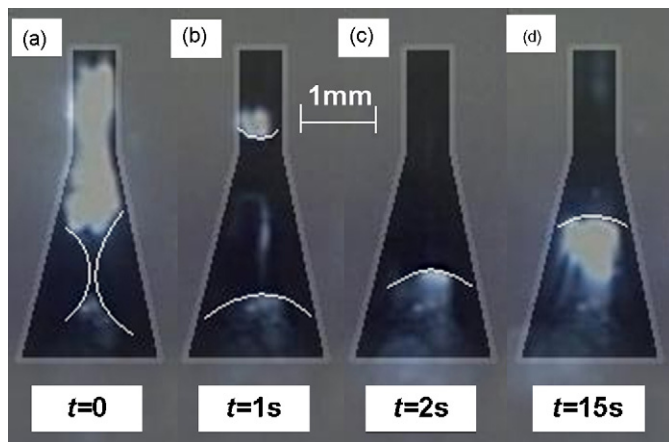


Fig. 10. Photograph of the water removal from the GDL in the fuel cell. Two droplets growing on opposite channel walls (a) merge and move upwards (b and c). After about 15 s, the main channel is cleared (d) ( $D = 4000 \mu\text{m}$ ;  $W = 2032 \mu\text{m}$ ;  $w = 300 \mu\text{m}$ ;  $2\alpha = 30^\circ$ ;  $\theta_1 = 15^\circ$ ;  $\theta_2 = 105^\circ$ ;  $j = 900 \text{ mA/cm}^2$ ;  $Bo = 0.14$ ).

### 4.3. Fuel cell experiments

The assembled fuel cell was run with class 5 hydrogen at the anode and ambient air at the cathode. A working point of 10 mbar air pressure and 50 mbar hydrogen pressure was set at a temperature of  $22^\circ\text{C}$ . The current was kept at  $900 \text{ mA/cm}^2$  using a current-controlled standard power supply (type PL330P from tti). This working point was found to support high liquid generation. Experiments were performed with pure graphite ( $\theta_1 = 60^\circ$ ) and the PEG-coated surface ( $\theta_1 \sim 15^\circ$ ).

### 4.4. Results and discussion

Capillary removal of liquid was observed for the PEG-coated channels for all studied opening angles ( $2\alpha = 15^\circ$ ,  $20^\circ$  and  $30^\circ$ ). Droplets formed on top of the GDL, which did soon attach to the hydrophilic channel walls and moved upward as soon as they got in contact with both channel walls (Fig. 10(a–c)).

Often, pairs of droplets were observed which grew very symmetric on opposite channel walls of the fuel cell as depicted in Fig. 10. The uplift started when two opposing droplets merged. Lift times for droplets varied from 1 to 15 s. In the previous experiments, droplet removal times in the PMMA test channels were larger than removal times in simulations but in the same range. In the fuel cell, however, the uplift times were decisively larger than expected from simulations. A possible explanation may be, that the simulations did not account for contact angle dynamics [17], which slow down the capillary movement. This effect was larger for the rougher surface of the graphite flow field. From Fig. 10, one can see that most of the time is required during the final stage of the removal process when the last part of the droplet moves into the secondary channel. This results from the decreasing capillary pressure difference and increasing viscous resistance in the secondary channel, which is successively filled. However, the time until the MEA/GDL surface is cleared, is still less than a second.

The uncoated graphite flow fields with the small opening angles of  $2\alpha = 15^\circ$  and  $20^\circ$  showed only poor performance as the liquid tended to pin at the corner where the tapered channel walls merge into the secondary removal channel. This demonstrates the relevance of the contact line hysteresis like discussed above.

The performance during the cold start ( $T = 22^\circ\text{C}$ ) of the cell, using the reference flow field and the flow field with tapered channels ( $2\alpha = 15^\circ$ ,  $20^\circ$  and  $30^\circ$ ,  $\theta_1 = 15^\circ$ ) is shown in Fig. 11. In the first few minutes, both configurations exhibit a decline in performance of about 15–20%. The power output of the reference cell decreases to 60% of the initial value in the following 15 min. The stepwise decline is correlated with observed sudden blocking events of two of the three channels of the flow field. In contrast, the cell with the tapered channels, regains its peak performance after about 10 min. The channels were never blocked completely, and droplets moved away from the GDL, as soon as they became large enough.

From the performance plot in Fig. 11, together with the observation of the flow field channels, it can be concluded that indeed, channel blocking led to the decrease in performance of the reference cell and the tapered flow field solved this problem.

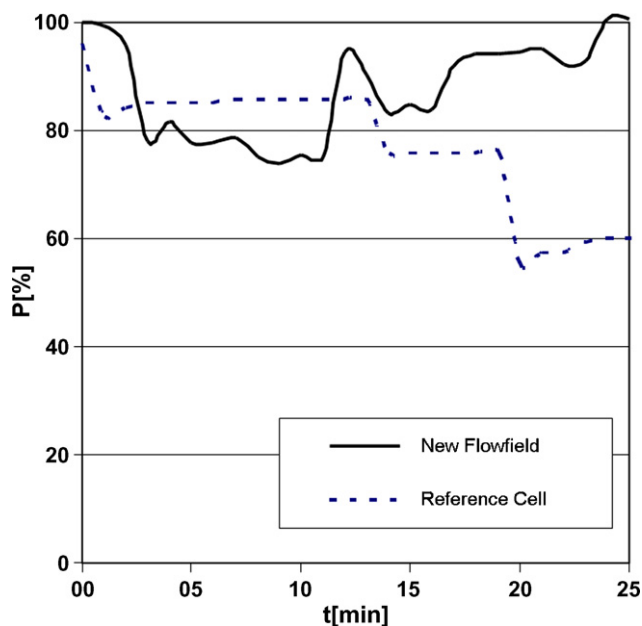


Fig. 11. Performance during cold start of the fuel cell with different flow field designs ( $j = 900 \text{ mA/cm}^2$ ).

## 5. Conclusion

A new type of droplet actuation has been proposed and applied to cathode flow fields of PEMFC. It enables passive removal of water from the active area of a fuel cell. The derived flow field design has been successfully validated by CFD simulations as well as by experiments within a fuel cell. From theory and experiments, it can be concluded that cathode walls with low contact angles and in particular low contact angle hysteresis as well as opening angles larger than  $2\alpha = 20^\circ$  are best suited to provide a safe water removal in realistic situations. The new channel design enables cost efficient PEMFCs without the need for external water removal components like pumps or similar. Furthermore, the proposed flow field enables a completely new class of channel designs, which do not require meandering arrangements, and can be optimized regarding humidification and oxygen supply without the concern of flooding.

## Acknowledgements

This work was funded by the German Science Foundation (DFG) within Project ZE 527/3 and the German Ministry of Education Project (BMBF) within 03SF0311B.

## References

[1] K. Tüber, Analyse des Betriebsverhaltens von Polymer-Elektrolyt-Membran-Brennstoffzellen für portable Systeme, Dissertation, Universität Duisburg-Essen, 2004.  
 [2] M. Müller, Polymermembran Brennstoffzellen mit mikrostrukturierten Strömungskanälen, Dissertation, University of Freiburg, 2002.  
 [3] T. Wüster, Entwicklung und Modellierung eines Polymerelektrolyt-Brennstoffzellenstapels der 5 kW Klasse, Dissertation, Forschungszentrums Jülich, 2005.

[4] F.Y. Zhang, X.G. Yang, C.Y. Wang, Liquid water removal from a polymer electrolyte fuel cell, *J. Electrochem. Soc.* 153 (2) (2006) A225–A232.  
 [5] Y. Wang, C.Y. Wang, Ultra large-scale simulation of polymer electrolyte fuel cells, *J. Power Sources* 153 (1) (2006) 130–135.  
 [6] H.C. Liu, W.M. Yan, C.Y. Soong, F. Chen, H.S. Chu, Reactant gas transport and cell performance of proton exchange membrane fuel cells with tapered flow field design, *J. Power Sources* 158 (1) (2006) 78–87.  
 [7] C. Litterst, S. Eccarius, C. Hebling, R. Zengerle, P. Koltay, Increasing  $\mu$ DMFC efficiency by passive CO<sub>2</sub> bubble removal and discontinuous operation, *J. Micromech. Microeng.* 16 (9) (2006) S248–S253.  
 [8] J. Kohnle, G. Waibel, R. Cernosa, M. Storz, H. Ernst, H. Sandmaier, T. Strobelt, R. Zengerle, A unique solution for preventing clogging of flow channels by gas bubbles, in: *IEEE MEMS, The 15th International IEEE Micro Electro Mechanical Conference ed Las Vegas, 2002*, pp. 77–80.  
 [9] T. Metz, N. Paust, C. Müller, R. Zengerle, P. Koltay, Micro structured flow field for passive water management in miniaturized PEM fuel cells, *Proc. of 20th IEEE MEMS (2007)* 863–866.  
 [10] N.T. Nguyen, S.T. Wereley, *Fundamentals and Applications of Microfluidics*, Artech House Books, Boston, 2002.  
 [11] D. Langbein, *Capillary Surfaces*, Springer-Verlag, 2002.  
 [12] P.G. de Gennes, Wetting: statics and dynamics, *Rev. Mod. Phys.* 57 (3) (1985) 827–863.  
 [13] R. Finn, *Equilibrium Capillary Surfaces*, Springer-Verlag, Stanford, 1986.  
 [14] ESI-CFD, *CFD-ACE+*, Modules Manual, Huntsville, 2006.  
 [15] SGL Carbon Group, <http://www.sglcarbon.com>.  
 [16] Baltic Fuel Cells GmbH, <http://www.balticfuelcells.de>.  
 [17] E.B. Dussan, Spreading of liquids on solid-surfaces—static and dynamic contact lines, *Annu. Rev. Fluid Mech.* 11 (1979) 371–400.

## Biographies

**Tobias Metz** studied geophysics at the University of Munich (Germany) with a major interest in numerical seismology; there he gained his diploma in 2003. In 2004, he was working as a research engineer at the Technical University of Munich in the field of computational fluid dynamics. He joined the Chair of Prof. Zengerle at the Institute for Microsystems Technology (IMTEK) as a PhD student in 2005. His main research interest is the field of capillary-driven movement of bubbles and droplets in microfluidic systems.

**Nils Paust** studied process engineering at the Technical University Berlin (Germany) where he gained his diploma in 2005. He joined the Chair of Prof. Zengerle at the Institute for Microsystem Technology (IMTEK) in 2006 as a PhD student. His main research interest is the simulation of bubbles and droplets in microfuel cells.

**Claas Müller** studied physics from 1986 to 1991 at the University of Karlsruhe. Following the physics diploma, he earned his doctorate in 1994 at the Forschungszentrum Karlsruhe, Institute for Micro Structure Technology, for his work on a miniaturized spectrometer system, fabricated by LIGA technology. Meanwhile, the microspectrometer is introduced to a broad range of industrial applications by the company microParts. At the Forschungszentrum, the prerequisites for a small-scale production were achieved. As a responsible project manager, Claas Müller was considerably involved in these activities. Since 1996, he is a graduate council at the Chair of Process Technology of the IMTEK. In 1999, he was appointed substitutional manager, and in 2004, the managing director of the Chair of Process Technology.

**Roland Zengerle** was born in 1965 and studied physics at the Technical University of Munich, Germany. From 1990 till 1995, he was a research engineer in the microactuator group at the Fraunhofer-Institute of Solid State Technology in Munich (today: FhG-IZM). Dr. Zengerle received his PhD degree from the “Universität der Bundeswehr” in Munich with the development of an electrostatically driven micropump. From 1995 till 1999, he was the head of the Microfluidics Department at Hahn-Schickard-Society (HSG-IMIT) in Villingen-Schwenningen, Germany. Since 1999, Dr. Zengerle is professor at the University of Freiburg, Germany. He is heading the IMTEK laboratory for MEMS Applications. This laboratory is a foundation of industry in order to stimulate the

cooperation between industry and university. The laboratory for MEMS Applications currently employs 30 research engineers and 10 master students. Since May 2005, Dr. Zengerle additionally is one of the new directors of HSG-IMIT in Villingen-Schwenningen. This institute currently employs 70 research engineers. The research focus of Dr. Zengerle is in the field of microfluidics and incorporates highly parallel sub-microliter dispensing techniques, miniaturized autonomous liquid handling systems, miniaturized and implantable drug delivery systems, lab-on-a-chip systems and micro- and nanofluidic simulation. Dr. Zengerle is a member of the International Steering Committee of the IEEE-MEMS Conference and was the past general Co-Chair of the MEMS 2006 conference taking place in Istanbul. He also serves on the programme committees of various international conferences like the IEEE-Transducers Conference, the International Conference on the Commercialization of Micro and Nano Sys-

tems (COMS), or the Actuator Conference. Dr. Zengerle is also the European Editor of the Springer journal “Microfluidics and Nanofluidics”.

**Peter Koltay** studied physics at the Universities of Freiburg (Germany) and Budapest (Hungary) and obtained his PhD from the University of Freiburg 1999 for his work on solar cells and photovoltaic modules. End of 1999, he joined the chair of Prof. Zengerle at the Institute for Microsystem Technology (IMTEK) of the University of Freiburg. There he is heading the pL & nL dispensers group and the group fluidic simulation. His research interests are especially related to the development of microfluidic liquid-handling devices for various life-science applications as, for example, microdispensers, modeling of free surface flows and simulation of microfluidic devices by system simulation and computational fluid dynamic simulation.